An FDTD TF-SF Boundary on Face-Centered Cubic Grids

Lijuan Shi [1], Lixia Yang [2], and Wei Feng [1]

[1] Department of Physics
Jiangsu University, Zhenjiang, 212013, China
juan-online@163.com, wfeng@ujs.edu.cn

[2] Department of Communication Engineering
Jiangsu University, Zhenjiang, 212013, China
lixiayang@yeah.net

Abstract ─ The implementation of total-field/scattered-field (TF-SF) boundary for finite-difference time-domain (FDTD) method was proposed based on face-centered cubic (FCC) grids. On the basis of the arrangement of fields components in the FCC voxel, the update equations for the electric and magnetic field components of the TF-SF boundary are derived. The resonant frequency of a cavity is calculated to illustrate that the FCC grid scheme is more accurate as compared to the equivalent Yee grid method. Then, by simulating the amplitude distribution of the vertical and oblique incident plane waves in the whole calculation region, the effectiveness of the TF-SF boundary is verified numerically.

Index Terms ─ Face-centered cubic grids, finite-difference time-domain method, total-field/scattered-field boundary.

I. INTRODUCTION

The finite-difference time-domain (FDTD) method is widely applied in many electromagnetic problems for its instinctive structure and simple implementation [1-6]. It is well known that the algorithmic structure of the standard FDTD method is based on Cartesian (Yee) grid [7,8]. However, due to the selection of computational molecule and grid, this Yee-based method has one drawback of anisotropy as described by the numerical dispersive equation. Thus, the wave-front distortions which would not appear in the analytic domain can be demonstrated in numerical simulations. One effective way of improving the isotropy of FDTD scheme is to use alternatives to the standard Cartesian grid [9-11]. Potter proposed the face-centered cubic (FCC) lattices for the discretization of Maxwell's equation [12]. The comparison of dispersion and stability analysis of this method with an equivalent Cartesian method has shown that the isotropy has been significantly improved, and the stability criterion has also been much relaxed than the Yee cell ($\Delta t|_{FCC} \approx 1.37473\Delta t|_{Yee}$), resulting in further computational savings. As a result, the FCC grid can be considered as an attractive alternative tesselation of 3D space for Maxwell's equations.

In order to apply the FDTD method based upon FCC grids to electromagnetic scattering problems of complex mediums, efficient total-field/scattered-field (TF-SF) boundary need to be introduced into the computation region [13,14]. The TF-SF formulation divides the entire FDTD lattice into two distinct regions. Incident and scattered fields exist in the total-field region, and scattered fields are only limited in the scattered-field region [15,16]. Failure to do so can lead to high levels of field leakage errors across the TF-SF boundary. In this paper, we present a detailed explanation of the implementation of TF-SF boundary for FDTD method based upon FCC grids.

The organization of this paper is as follows: Section 2 simply introduces the FCC grid structure. In Section 3, the update equations for the electric and magnetic field components of the TF-SF boundary are derived. The effectiveness of the proposed scheme is numerically verified in Section 4. Section 5 are the conclusions.

II. DESCRIPTION OF THE FCC GRID STRUCTURE

The face-centered cubic (FCC) grid is a spatial extension of hexagonal grid. The arrangement of electric and magnetic fields in the FCC voxel is shown in Fig. 1, which consists of lattice points lying at each corner and in the center of all six faces [5]. Two FCC grids should be considered for discretizing Maxwell's equations: one indicates the electric field components, and the other hosts the magnetic components. Different from the conventional Cartesian (Yee) grid, both electric field components and magnetic field components are collocated (each lattice point denote all three components) in FCC grids, whereas magnetic and electric fields are

Submitted On: August 6, 2019
Accepted On: April 12, 2020

staggered. It is obviously seen that there are four unique electric field vectors and four unique magnetic field vectors in the FCC voxel: located at the closest corners, as well as lying in the center of the xy-face, yz-face and xz-face. For the purposes of indexing and analysis, the side lengths of the FCC voxel are assumed as $\Delta x, \Delta y$ and Δz, the indies with a given voxel are set as $(i, j, k, n) = (i\Delta x, j\Delta y, k\Delta z, n\Delta t)$, where Δt is the time step. The magnetic field grid is displaced from the electric field grid along the direction of the voxel main diagonal by the displacement vector $d = (\Delta x/4, \Delta y/4, \Delta z/4)$.

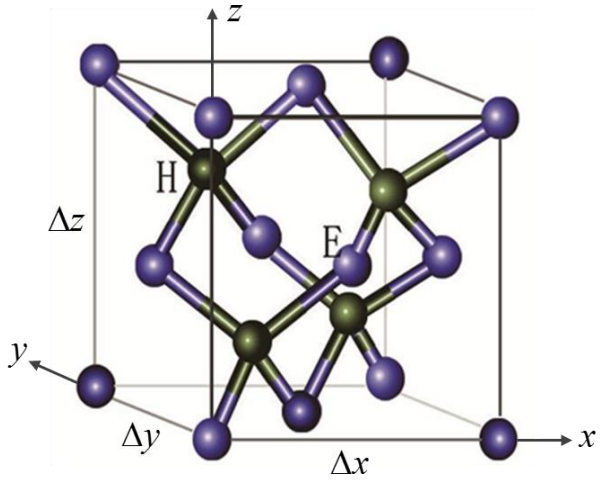

Fig. 1. Electric and magnetic field lattice points in the FCC voxel.

According to the arrangement of fields components in the FCC voxel, the tetrahedral structure of electric fields surrounding a given magnetic field is shown in Fig. 2 (a). The field update equations at the tetrahedron center are obtained using these nearest neighbors. Projecting this tetrahedral structure onto the rectangular coordinate axes, the displacement vectors that represent the location of these electric field components with reference to the magnetic field location, are $\boldsymbol{e}_1 = \left(-\frac{\Delta x}{4}, \frac{\Delta y}{4}, \frac{\Delta z}{4}\right)$, $\boldsymbol{e}_2 = \left(\frac{\Delta x}{4}, -\frac{\Delta y}{4}, \frac{\Delta z}{4}\right)$, $\boldsymbol{e}_3 = \left(\frac{\Delta x}{4}, \frac{\Delta y}{4}, -\right)$, and $\boldsymbol{e}_4 = \left(-\frac{\Delta x}{4}, -\frac{\Delta y}{4}, -\frac{\Delta z}{4}\right)$, respectively. On the contrary, in Fig. 2 (b) the appropriate displacement vectors presenting the magnetic field locations neighboring the electric field, are $\boldsymbol{h}_1 = \left(\frac{\Delta x}{4}, \frac{\Delta y}{4}, \frac{\Delta z}{4}\right)$, $\boldsymbol{h}_2 = \left(-\frac{\Delta x}{4}, -\frac{\Delta y}{4}, \frac{\Delta z}{4}\right)$, $\boldsymbol{h}_3 = \left(-\frac{\Delta x}{4}, \frac{\Delta y}{4}, -\frac{\Delta z}{4}\right)$ and $\boldsymbol{h}_4 = \left(\frac{\Delta x}{4}, -\frac{\Delta y}{4}, -\frac{\Delta z}{4}\right)$, respectively.

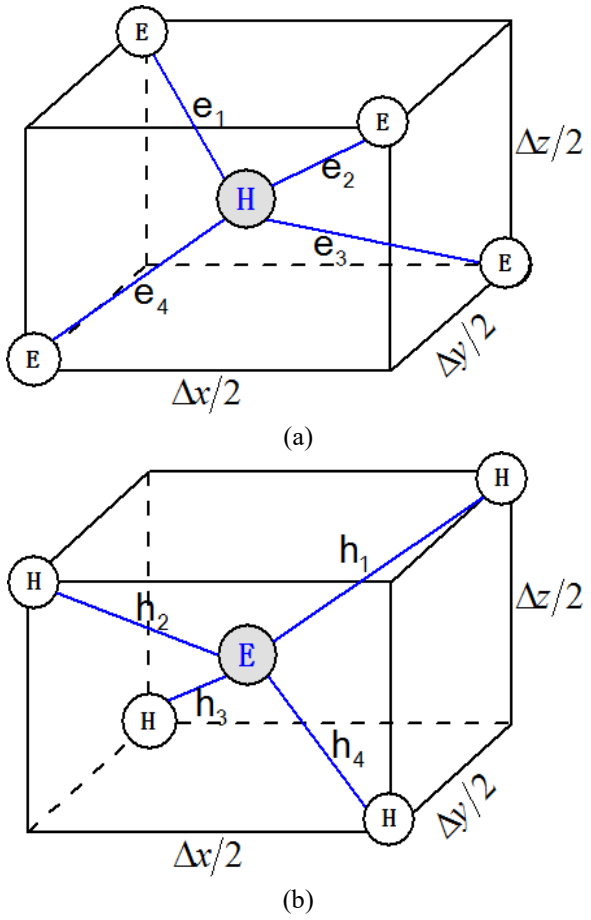

Fig. 2. (a) The organization of the electric fields neighboring a specified magnetic field point; and (b) the organization of the magnetic fields neighboring a specified electric field point.

III. TF-SF BOUNDARY IMPLEMENTATION ON FCC GRIDS

As illustrated in Fig. 3 (a), the field update points around the TF-SF boundary for the FDTD method on FCC grids are different from those on the Yee scheme. The field update points on the TF-SF boundary are assumed as electric field grids, and the grid points displace $\Delta_m/4$ ($m \in x, y, z$) away from the TF/SF boundary are set as magnetic field grids. Here, we take the upper boundary as an example. The derivations for other five boundary proceeds in a similar way. In Fig. 3 (b), the filled circle ② at the upper boundary indicates the electric field grid located at the corners of FCC grids, and circles ① and ③ indicate electric field grid lying in the center of the face of an FCC grid. The hollow circles ④-⑦ indicate the neighboring magnetic field grids on the exterior boundary located $\Delta_z/4$ distance away from the upper boundary.

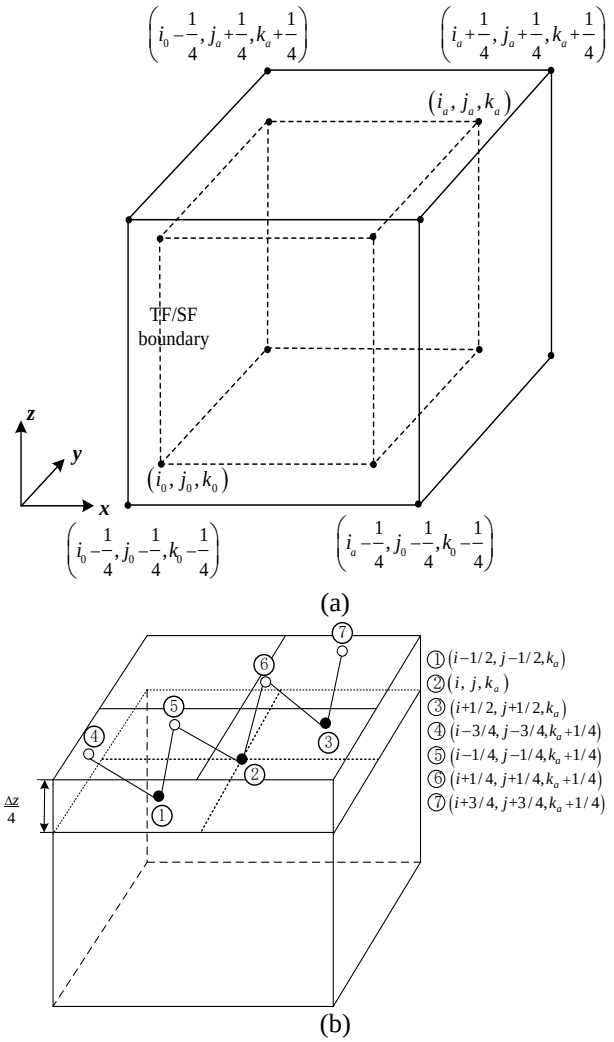

Fig. 3. (a)TF-SF field boundary of FCC-FDTD method; and (b) arrangement of fields components at the upper boundary.

A. Update equations of electric field components

It is obvious that the computations of the electric field components on the TF-SF boundary are related to the magnetic field components on the exterior boundary which belong to the SF field. Therefore, when the incident wave is introduced into TF region by the TF-SF boundary, the iteration equations of electric field components are required to add the incident wave field value at the corresponding time step and the grid [1]. Thus, the update equations of electric field components at the upper boundary ($z = z_a$) can be obtained as below:

(1) Electric field grid located at the corners of FCC grids:

$$E_x\big|_{i,j,k_a}^{n+1} = \left\{E_x\big|_{i,j,k_a}^{n+1}\right\}_{FCC} + \frac{\Delta t}{\Delta y\cdot\varepsilon}\left[H_{z,i}\big|_{i+\frac14,j+\frac14,k_a+\frac14}^{n+1/2} - H_{z,i}\big|_{i-\frac14,j-\frac14,k_a+\frac14}^{n+1/2}\right] - \frac{\Delta t}{\Delta z\cdot\varepsilon}\left[H_{y,i}\big|_{i+\frac14,j+\frac14,k_a+\frac14}^{n+1/2} + H_{y,i}\big|_{i-\frac14,j-\frac14,k_a+\frac14}^{n+1/2}\right], \quad (1)$$

where $\left\{E_x\big|_{i,j,k_a}^{n+1}\right\}_{FCC}$ is update equation for electric component E_x at location (i, j, k_a) based upon FCC grids:

$$\left\{E_x\big|_{i,j,k_a}^{n+1}\right\}_{FCC} = E_x\big|_{i,j,k_a}^{n} + \frac{\Delta t}{\Delta y\cdot\varepsilon}\left[H_z\big|_{i+\frac14,j+\frac14,k_a+\frac14}^{n+1/2} + H_z\big|_{i-\frac14,j+\frac14,k_a-\frac14}^{n+1/2} - H_z\big|_{i+\frac14,j-\frac14,k_a+\frac14}^{n+1/2} - H_z\big|_{i+\frac14,j-\frac14,k_a-\frac14}^{n+1/2}\right] - \frac{\Delta t}{\Delta z\cdot\varepsilon}\left[H_y\big|_{i+\frac14,j+\frac14,k_a+\frac14}^{n+1/2} + H_y\big|_{i-\frac14,j-\frac14,k_a+\frac14}^{n+1/2} - H_y\big|_{i+\frac14,j+\frac14,k_a-\frac14}^{n+1/2} - H_y\big|_{i-\frac14,j-\frac14,k_a-\frac14}^{n+1/2}\right]. \quad (2)$$

Similarly, the update equations can be obtained for $E_y\big|_{i,j,k_a}^{n+1}$ and $E_z\big|_{i,j,k_a}^{n+1}$,

$$E_y\big|_{i,j,k_a}^{n+1} = \left\{E_y\big|_{i,j,k_a}^{n+1}\right\}_{FCC} + \frac{\Delta t}{\Delta z\cdot\varepsilon}\left[H_{x,i}\big|_{i+\frac14,j+\frac14,k_a+\frac14}^{n+1/2} + H_{x,i}\big|_{i-\frac14,j-\frac14,k_a+\frac14}^{n+1/2}\right] - \frac{\Delta t}{\Delta x\cdot\varepsilon}\left[H_{z,i}\big|_{i+\frac14,j+\frac14,k_a+\frac14}^{n+1/2} - H_{z,i}\big|_{i-\frac14,j-\frac14,k_a+\frac14}^{n+1/2}\right], \quad (3)$$

$$E_z\big|_{i,j,k_a}^{n+1} = \left\{E_z\big|_{i,j,k_a}^{n+1}\right\}_{FCC} + \frac{\Delta t}{\Delta x\cdot\varepsilon}\left[H_{y,i}\big|_{i+\frac14,j+\frac14,k_a+\frac14}^{n+1/2} - H_{y,i}\big|_{i-\frac14,j-\frac14,k_a+\frac14}^{n+1/2}\right] - \frac{\Delta t}{\Delta y\cdot\varepsilon}\left[H_{x,i}\big|_{i+\frac14,j+\frac14,k_a+\frac14}^{n+1/2} + H_{x,i}\big|_{i-\frac14,j-\frac14,k_a+\frac14}^{n+1/2}\right], \quad (4)$$

where

$$\left\{E_y\big|_{i,j,k_a}^{n+1}\right\}_{FCC} = E_y\big|_{i,j,k_a}^{n} + \frac{\Delta t}{\Delta z\cdot\varepsilon}\left[H_x\big|_{i+\frac14,j+\frac14,k_a+\frac14}^{n+1/2} + H_x\big|_{i-\frac14,j-\frac14,k_a+\frac14}^{n+1/2} - H_x\big|_{i-\frac14,j+\frac14,k_a-\frac14}^{n+1/2} - H_x\big|_{i+\frac14,j-\frac14,k_a-\frac14}^{n+1/2}\right] - \frac{\Delta t}{\Delta x\cdot\varepsilon}\left[H_z\big|_{i+\frac14,j+\frac14,k_a+\frac14}^{n+1/2} + H_z\big|_{i+\frac14,j-\frac14,k_a-\frac14}^{n+1/2} - H_z\big|_{i-\frac14,j+\frac14,k_a+\frac14}^{n+1/2} - H_z\big|_{i-\frac14,j-\frac14,k_a-\frac14}^{n+1/2}\right], \quad (5)$$

$$\left\{E_z\Big|_{i,j,k_a}^{n+1}\right\}_{FCC}=E_z\Big|_{i,j,k_a}^{n}+\frac{\Delta t}{\Delta x\cdot\varepsilon}\left[H_y\Big|_{i+\frac{1}{4},j+\frac{1}{4},k_a+\frac{1}{4}}^{n+1/2}+H_y\Big|_{i+\frac{1}{4},j-\frac{1}{4},k_a-\frac{1}{4}}^{n+1/2}-H_y\Big|_{i-\frac{1}{4},j-\frac{1}{4},k_a+\frac{1}{4}}^{n+1/2}-H_z\Big|_{i-\frac{1}{4},j+\frac{1}{4},k_a-\frac{1}{4}}^{n+1/2}\right]-\frac{\Delta t}{\Delta y\cdot\varepsilon}\left[H_x\Big|_{i+\frac{1}{4},j+\frac{1}{4},k_a+\frac{1}{4}}^{n+1/2}+H_x\Big|_{i-\frac{1}{4},j+\frac{1}{4},k_a-\frac{1}{4}}^{n+1/2}-H_x\Big|_{i-\frac{1}{4},j-\frac{1}{4},k_a+\frac{1}{4}}^{n+1/2}-H_x\Big|_{i+\frac{1}{4},j-\frac{1}{4},k_a-\frac{1}{4}}^{n+1/2}\right]. \tag{6}$$

In addition, for the electric field components located at four edges of the upper boundary, they also belong to the corners of FCC grids, and can be derived in the same way.

(2) Electric field grid lying in the center of the face of FCC grids:

$$E_x\Big|_{i+\frac{1}{2},j+\frac{1}{2},k_a}^{n+1}=\left\{E_x\Big|_{i+\frac{1}{2},j+\frac{1}{2},k_a}^{n+1}\right\}_{FCC}+\frac{\Delta t}{\Delta y\cdot\varepsilon}\left[H_{z,i}\Big|_{i+\frac{3}{4},j+\frac{3}{4},k_a+\frac{1}{4}}^{n+1/2}-H_{z,i}\Big|_{i+\frac{1}{4},j+\frac{1}{4},k_a+\frac{1}{4}}^{n+1/2}\right]-\frac{\Delta t}{\Delta z\cdot\varepsilon}\left[H_{y,i}\Big|_{i+\frac{3}{4},j+\frac{3}{4},k_a+\frac{1}{4}}^{n+1/2}+H_{y,i}\Big|_{i+\frac{1}{4},j+\frac{1}{4},k_a+\frac{1}{4}}^{n+1/2}\right], \tag{7}$$

$$E_y\Big|_{i+\frac{1}{2},j+\frac{1}{2},k_a}^{n+1}=\left\{E_y\Big|_{i+\frac{1}{2},j+\frac{1}{2},k_a}^{n+1}\right\}_{FCC}+\frac{\Delta t}{\Delta z\cdot\varepsilon}\left[H_{x,i}\Big|_{i+\frac{3}{4},j+\frac{3}{4},k_a+\frac{1}{4}}^{n+1/2}-H_{x,i}\Big|_{i+\frac{1}{4},j+\frac{1}{4},k_a+\frac{1}{4}}^{n+1/2}\right]-\frac{\Delta t}{\Delta x\cdot\varepsilon}\left[H_{z,i}\Big|_{i+\frac{3}{4},j+\frac{3}{4},k_a+\frac{1}{4}}^{n+1/2}+H_{z,i}\Big|_{i+\frac{1}{4},j+\frac{1}{4},k_a+\frac{1}{4}}^{n+1/2}\right], \tag{8}$$

$$E_z\Big|_{i+\frac{1}{2},j+\frac{1}{2},k_a}^{n+1}=\left\{E_z\Big|_{i+\frac{1}{2},j+\frac{1}{2},k_a}^{n+1}\right\}_{FCC}+\frac{\Delta t}{\Delta x\cdot\varepsilon}\left[H_{y,i}\Big|_{i+\frac{3}{4},j+\frac{3}{4},k_a+\frac{1}{4}}^{n+1/2}-H_{y,i}\Big|_{i+\frac{1}{4},j+\frac{1}{4},k_a+\frac{1}{4}}^{n+1/2}\right]-\frac{\Delta t}{\Delta y\cdot\varepsilon}\left[H_{x,i}\Big|_{i+\frac{3}{4},j+\frac{3}{4},k_a+\frac{1}{4}}^{n+1/2}+H_{x,i}\Big|_{i+\frac{1}{4},j+\frac{1}{4},k_a+\frac{1}{4}}^{n+1/2}\right]. \tag{9}$$

Here, $\left\{E_y\Big|_{i+\frac{1}{2},j+\frac{1}{2},k_a}^{n+1}\right\}_{FCC}$, $\left\{E_y\Big|_{i+\frac{1}{2},j+\frac{1}{2},k_a}^{n+1}\right\}_{FCC}$ and $\left\{E_y\Big|_{i+\frac{1}{2},j+\frac{1}{2},k_a}^{n+1}\right\}_{FCC}$ in equations (7-9) are the update equations of electric field components at node $\left\{i+\frac{1}{2},j_0,k+\frac{1}{2}\right\}$, which can be easily obtained by replacing $\{i,j,k_a\}$ in equations (2), (5) and (6) with $\left\{i+\frac{1}{2},j_0,k+\frac{1}{2}\right\}$, respectively .

B. Update equations of magnetic field components

In Fig. 3, it is also seen that the computations of magnetic field components on the exterior boundary located $\Delta_z/4$ distance away from the upper boundary are related to the electric field components on the TF-SF boundary, and therefore the iteration equations of magnetic field components are required to subtract the incident wave field value at the corresponding the grid on the TF-SF boundary. Then, the update equations of magnetic field components can be represented as below:

(1) Magnetic field grid located at the corners of FCC grids:

$$H_x\Big|_{i+\frac{1}{4},j+\frac{1}{4},k_a+\frac{1}{4}}^{n+1/2}=\left\{H_x\Big|_{i+\frac{1}{4},j+\frac{1}{4},k_a+\frac{1}{4}}^{n+1/2}\right\}_{FCC}+\frac{\Delta t}{\Delta z\cdot\mu}\left[E_{y,i}\Big|_{i+\frac{1}{2},j+\frac{1}{2},k_a}^{n}+E_{y,i}\Big|_{i,j,k_a}^{n}\right]+\frac{\Delta t}{\Delta y\cdot\mu}\left[E_{z,i}\Big|_{i+\frac{1}{2},j+\frac{1}{2},k_a}^{n}-E_{z,i}\Big|_{i,j,k_a}^{n}\right], \tag{10}$$

$$H_y\Big|_{i+\frac{1}{4},j+\frac{1}{4},k_a+\frac{1}{4}}^{n+1/2}=\left\{H_y\Big|_{i+\frac{1}{4},j+\frac{1}{4},k_a+\frac{1}{4}}^{n+1/2}\right\}_{FCC}-\frac{\Delta t}{\Delta x\cdot\mu}\left[E_{z,i}\Big|_{i+\frac{1}{2},j+\frac{1}{2},k_a}^{n}-E_{z,i}\Big|_{i,j,k_a}^{n}\right]-\frac{\Delta t}{\Delta z\cdot\mu}\left[E_{x,i}\Big|_{i+\frac{1}{2},j+\frac{1}{2},k_a}^{n}+E_{x,i}\Big|_{i,j,k_a}^{n}\right], \tag{11}$$

$$H_z\Big|_{i+\frac{1}{4},j+\frac{1}{4},k_a+\frac{1}{4}}^{n+1/2}=\left\{H_z\Big|_{i+\frac{1}{4},j+\frac{1}{4},k_a+\frac{1}{4}}^{n+1/2}\right\}_{FCC}-\frac{\Delta t}{\Delta y\cdot\mu}\left[E_{x,i}\Big|_{i+\frac{1}{2},j+\frac{1}{2},k_a}^{n}-E_{x,i}\Big|_{i,j,k_a}^{n}\right]+\frac{\Delta t}{\Delta x\cdot\mu}\left[E_{y,i}\Big|_{i+\frac{1}{2},j+\frac{1}{2},k_a}^{n}-E_{y,i}\Big|_{i,j,k_a}^{n}\right], \tag{12}$$

where $\left\{H_x\Big|_{i+\frac{1}{4},j+\frac{1}{4},k_a+\frac{1}{4}}^{n+1/2}\right\}_{FCC}$, $\left\{H_y\Big|_{i+\frac{1}{4},j+\frac{1}{4},k_a+\frac{1}{4}}^{n+1/2}\right\}_{FCC}$ and $\left\{H_z\Big|_{i+\frac{1}{4},j+\frac{1}{4},k_a+\frac{1}{4}}^{n+1/2}\right\}_{FCC}$ are the update equations of magnetic field components at location $\left\{i+\frac{1}{4},j+\frac{1}{4},k_a+\frac{1}{4}\right\}$ based upon FCC grids:

$$\left\{H_x\Big|_{i+\frac{1}{4},j+\frac{1}{4},k_a+\frac{1}{4}}^{n+1/2}\right\}_{FCC}=H_x\Big|_{i+\frac{1}{4},j+\frac{1}{4},k_a+\frac{1}{4}}^{n-1/2}+\frac{\Delta t}{\Delta z\cdot\mu}\left[E_y\Big|_{i,j+\frac{1}{2},k_a+\frac{1}{2}}^{n}+E_y\Big|_{i+\frac{1}{2},j,k_a+\frac{1}{2}}^{n}-E_y\Big|_{i+\frac{1}{2},j+\frac{1}{2},k_a}^{n}-E_y\Big|_{i,j,k_a}^{n}\right]-\frac{\Delta t}{\Delta y\cdot\mu}\left[E_z\Big|_{i,j+\frac{1}{2},k_a+\frac{1}{2}}^{n}+E_z\Big|_{i+\frac{1}{2},j+\frac{1}{2},k_a}^{n}-E_z\Big|_{i+\frac{1}{2},j,k_a+\frac{1}{2}}^{n}-E_z\Big|_{i,j,k_a}^{n}\right], \tag{13}$$

$$\left\{H_y\Big|_{i+\frac{1}{4},j+\frac{1}{4},k_a+\frac{1}{4}}^{n+1/2}\right\}_{FCC} = H_y\Big|_{i+\frac{1}{4},j+\frac{1}{4},k_a+\frac{1}{4}}^{n-1/2} + \frac{\Delta t}{\Delta x\cdot\mu}\left[E_z\Big|_{i+\frac{1}{2},j,k_a+\frac{1}{2}}^{n} + E_z\Big|_{i+\frac{1}{2},j+\frac{1}{2},k_a}^{n} - E_z\Big|_{i,j+\frac{1}{2},k_a+\frac{1}{2}}^{n} - E_z\Big|_{i,j,k_a}^{n}\right] - \frac{\Delta t}{\Delta z\cdot\mu}\left[E_x\Big|_{i,j+\frac{1}{2},k_a+\frac{1}{2}}^{n} + E_x\Big|_{i+\frac{1}{2},j,k_a+\frac{1}{2}}^{n} - E_x\Big|_{i+\frac{1}{2},j+\frac{1}{2},k_a}^{n} - E_x\Big|_{i,j,k_a}^{n}\right], \quad (14)$$

$$\left\{H_z\Big|_{i+\frac{1}{4},j+\frac{1}{4},k_a+\frac{1}{4}}^{n+1/2}\right\}_{FCC} = H_z\Big|_{i+\frac{1}{4},j+\frac{1}{4},k_a+\frac{1}{4}}^{n-1/2} + \frac{\Delta t}{\Delta y\cdot\mu}\left[E_x\Big|_{i,j+\frac{1}{2},k_a+\frac{1}{2}}^{n} + E_x\Big|_{i+\frac{1}{2},j+\frac{1}{2},k_a}^{n} - E_x\Big|_{i,j,k_a+\frac{1}{2}}^{n} - E_x\Big|_{i+\frac{1}{2},j,k_a}^{n}\right] - \frac{\Delta t}{\Delta x\cdot\mu}\left[E_y\Big|_{i+\frac{1}{2},j,k_a+\frac{1}{2}}^{n} + E_y\Big|_{i+\frac{1}{2},j+\frac{1}{2},k_a}^{n} - E_y\Big|_{i,j+\frac{1}{2},k_a+\frac{1}{2}}^{n} - E_y\Big|_{i,j,k_a}^{n}\right]. \quad (15)$$

(2) Magnetic field grid lying in the center of the face of FCC grids:

$$H_x\Big|_{i+\frac{3}{4},j+\frac{3}{4},k_a+\frac{1}{4}}^{n+1/2} = \left\{H_x\Big|_{i+\frac{3}{4},j+\frac{3}{4},k_a+\frac{1}{4}}^{n+1/2}\right\}_{FCC} + \frac{\Delta t}{\Delta z\cdot\mu}\left[E_{y,i}\Big|_{i+1,j+1,k_a}^{n} + E_{y,i}\Big|_{i+\frac{1}{2},j+\frac{1}{2},k_a}^{n}\right] + \frac{\Delta t}{\Delta y\cdot\mu}\left[E_{z,i}\Big|_{i+1,j+1,k_a}^{n} - E_{z,i}\Big|_{i+\frac{1}{2},j+\frac{1}{2},k_a}^{n}\right], \quad (16)$$

$$H_y\Big|_{i+\frac{3}{4},j+\frac{3}{4},k_a+\frac{1}{4}}^{n+1/2} = \left\{H_y\Big|_{i+\frac{3}{4},j+\frac{3}{4},k_a+\frac{1}{4}}^{n+1/2}\right\}_{FCC} - \frac{\Delta t}{\Delta x\cdot\mu}\left[E_{z,i}\Big|_{i+1,j+1,k_a}^{n} - E_{z,i}\Big|_{i+\frac{1}{2},j+\frac{1}{2},k_a}^{n}\right] - \frac{\Delta t}{\Delta z\cdot\mu}\left[E_{x,i}\Big|_{i+1,j+1,k_a}^{n} + E_{x,i}\Big|_{i+\frac{1}{2},j+\frac{1}{2},k_a}^{n}\right], \quad (17)$$

$$H_z\Big|_{i+\frac{3}{4},j+\frac{3}{4},k_a+\frac{1}{4}}^{n+1/2} = \left\{H_z\Big|_{i+\frac{3}{4},j+\frac{3}{4},k_a+\frac{1}{4}}^{n+1/2}\right\}_{FCC} - \frac{\Delta t}{\Delta y\cdot\mu}\left[E_{x,i}\Big|_{i+1,j+1,k_a}^{n} - E_{x,i}\Big|_{i+\frac{1}{2},j+\frac{1}{2},k_a}^{n}\right] + \frac{\Delta t}{\Delta x\cdot\mu}\left[E_{y,i}\Big|_{i+1,j+1,k_a}^{n} - E_{y,i}\Big|_{i+\frac{1}{2},j+\frac{1}{2},k_a}^{n}\right], \quad (18)$$

where $\left\{H_x\Big|_{i+\frac{3}{4},j+\frac{3}{4},k_a+\frac{1}{4}}^{n+1/2}\right\}_{FCC}$, $\left\{H_y\Big|_{i+\frac{3}{4},j+\frac{3}{4},k_a+\frac{1}{4}}^{n+1/2}\right\}_{FCC}$ and $\left\{H_z\Big|_{i+\frac{3}{4},j+\frac{3}{4},k_a+\frac{1}{4}}^{n+1/2}\right\}_{FCC}$ are the update equations of magnetic field components at location $\left\{i+\frac{3}{4}, j+\frac{3}{4}, k_a+\frac{1}{4}\right\}$ based upon FCC grids, respectively.

IV. NUMERICAL RESULTS

In this section, we will first validate update equations for the electric and magnetic field component reformulated on FCC grids, as the implementation of the proposed TF-SF boundary for the FDTD method are based on these update equations. Here, let us consider an empty rectangular metal cavity. The cavity size is $10mm\times15mm\times16mm$. The FCC cell sizes are $\delta=\Delta x=\Delta y=\Delta z=0.5mm$. The time step is $\Delta t=\delta/2.5c_0$=0.667 ps, where c_0 is the speed of light in vacuum. A modulated Gaussian pulse is used as the source function, which is described by:

$$P(t)=\exp[-4\pi(t-t_0)^2/\tau^2]\times\cos(\omega t), \quad (19)$$

with the angular frequency parameter ω=$4\pi\times10^{10}$, delay parameter τ=30Δt and $t_0=0.8\tau$. The excitation source is placed at (0,0,0). Figure 4 plots the waveform of E_z component of TM_{111} mode at observation point (0,0,10). The simulated results demonstrate the convergence of the proposed FCC grid method. In Fig. 5, the resonant frequency of TM_{111} mode of the cavity using the FCC method is 20.086GHz, and the theoretical resonant frequency of the cavity is 20.319GHz. The structure is also simulated in the standard Cartesian grids using the same cell sizes, and the resulting resonant frequency is 19.932GHz. The relative error is defined as $\delta_E=\left|(f_0-f_r)/f_0\right|\times100\%$, where f_0 is analytical frequency of the cavity, f_r is the simulation frequency of the cavity. The relative error obtained by FCC method and Cartesian method are 1.147% and 1.904%, respectively. It is shown that the FCC grid code is more accurate as compared to the traditional Yee grid method.

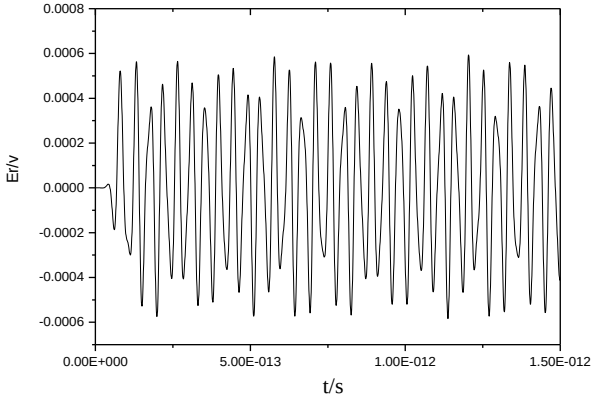

Fig. 4. E_z component of TM_{111} mode at observation point (0,0,10).

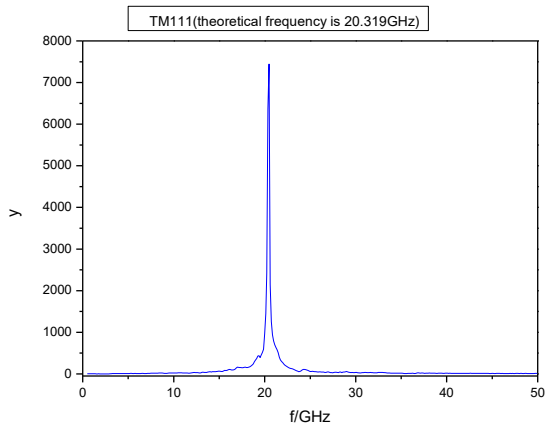

Fig. 5. The resonant frequency of TM_{111} mode of the cavity based upon the FCC grids.

Next, numerical examples are presented to validate the proposed TF-SF boundary for a plane wave excitation in the FDTD scheme based upon FCC grids. Here, a sinusoidal wave as an incident source is expressed by:

$$f = \sin(2\pi c_0 t / \lambda), \tag{20}$$

where c_0 is the speed of light in vacuum, and the wavelength of plane wave is λ=0.1m . The total computational region contains $280\times280\times280$ FCC cells with 280 cells along x, y and z directions, respectively. The TF region has 60 FCC cells along x, y and z directions, respectively. The spatial step is set as $\delta = \Delta x = \Delta y = \Delta z = 5\times10^{-3} m$, and the time step size is $\Delta t = \delta / 4c_0$=4.17 ps . The calculation program was set to run 1000 time steps. Numerical results in Fig. 6 are for the case of vertical incidence. Figures 6 (a) and 6 (b) show the plane wave amplitude distribution in the yz-plane section of the TF area at time step $220\Delta t$ and $380\Delta t$, respectively. The value of the right color bar indicates the relative amplitude value of E_x . The E_x field value against time at the observation point (0,0,0) is shown in Fig. 6 (c). It is clearly seen that there are no field leakage errors across the TF-SF boundary. The incident wave is successfully introduced into the TF area with the proposed TF-SF boundary.

Finally, the effectiveness of this TF-SF boundary for introducing plane wave at oblique incidence will be verified. The plane wave amplitude distribution in the yz-plane section of the TF area at time step $t = 220\Delta t$ and $t = 440\Delta t$ are shown in Fig. 7 (a) and Fig. 7 (b), respectively. Figure 7 (c) plots the E_x field value against time at the observation point (0,0,0). It is further shown that the incident wave is successfully introduced into the TF area efficiently with the proposed TF-SF boundary. It therefore appears that this study lays a solid foundation for using FDTD method based on FCC grids to deal with scattering problems. In Figs. 6 (c) and 7 (c), we found that the value of electric field varies slightly with the increase of time. This is due to the fact that the computational domain wasn't truncated by the absorption boundary. There are certain reflections from the computational boundary. The related absorbing boundary conditions for FDTD method based upon FCC grid will be studied in future work.

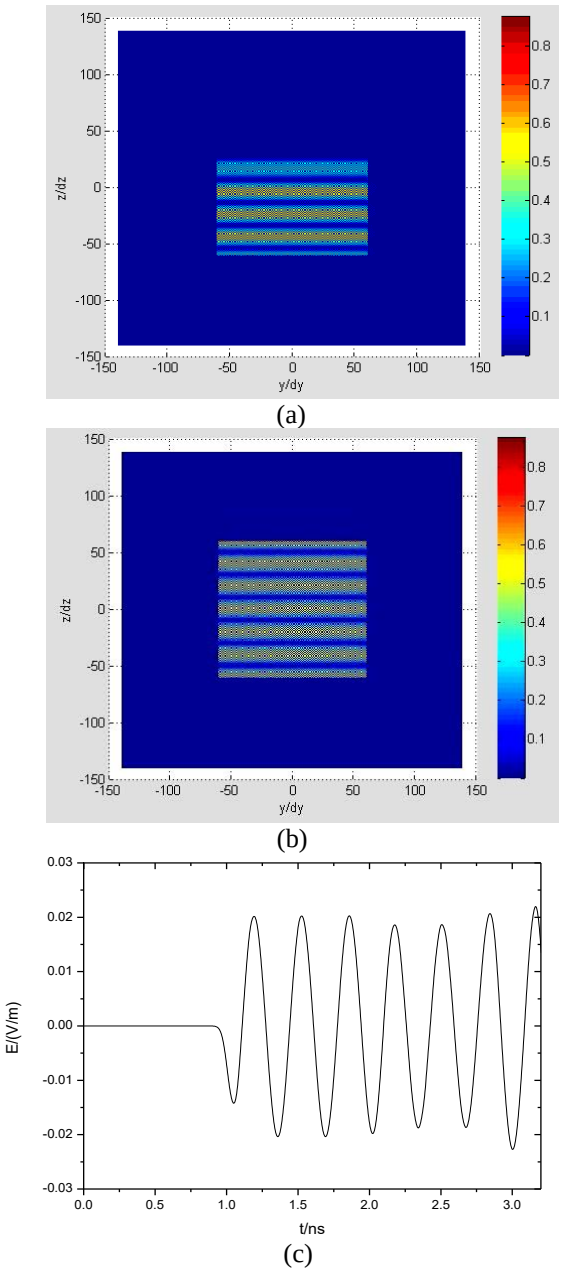

Fig. 6. Plane wave introduced into the TF area at vertical incidence: (a) amplitude distribution of electric component E_x at time step $t = 220\Delta t$; (b) amplitude distribution of electric component E_x at the time $t = 380\Delta t$; (c) field value of E_x against time at the observation point (0,0,0).

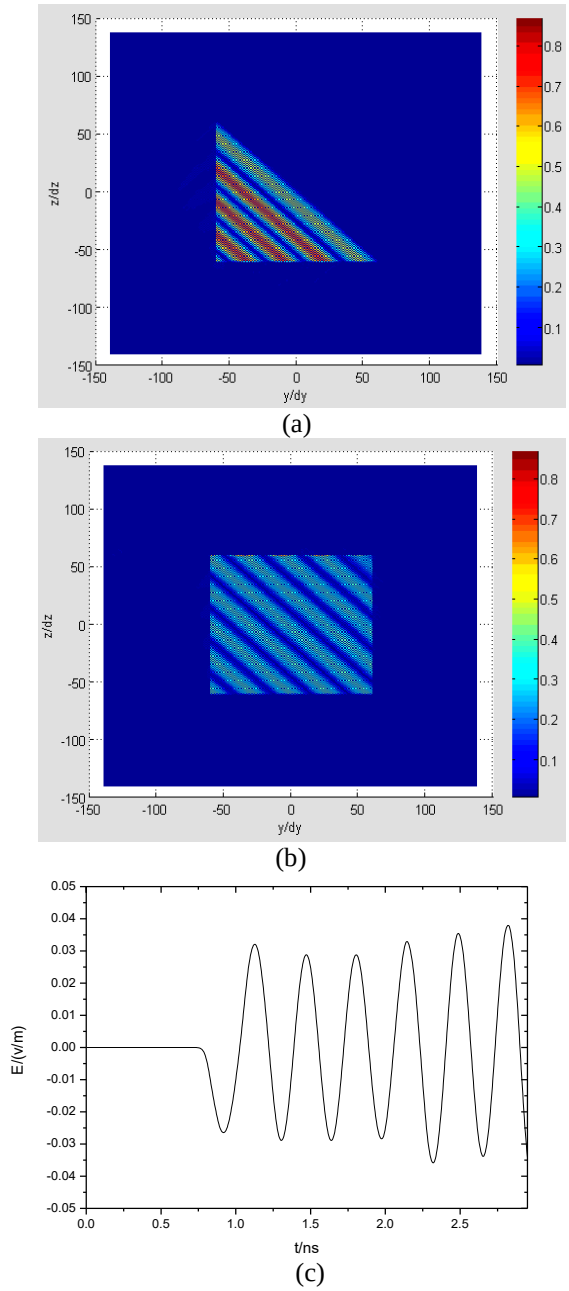

Fig. 7. Plane wave introduced into the TF area at vertical incidence: (a) amplitude distribution of electric component E_x at time step $t = 220\Delta t$; (b) amplitude distribution of electric component E_x at the time $t = 380\Delta t$; (c) field value of E_x against time at the observation point (0,0,0).

VI. CONCLUSION

In this paper, we formulate an effective TF-SF technique for the FDTD method based upon FCC grids is presented. According to the location of electric and magnetic field components in the FCC voxel, the difference iteration formulas for the electric and magnetic field components of the upper boundary are derived. Numerical results demonstrate that the incident plane wave can be successfully introduced into the TF area with the proposed TF-SF boundary. Future work will establish the complete FCC-FDTD algorithm for the EM scattering of targets by researching on the related absorbing boundary conditions and the near-to-far field transformation boundary.

ACKNOWLEDGMENT

This paper is supported by the National Natural Science Foundation of China (Grant No. 61601205, No. 11604126), Basic Research Program of Jiangsu Province (Natural Science Foundation for Young Scholars) (Grant No. BK20160541), and the Natural Science Foundation of the Jiangsu Higher Education Institutions of China (Grant No. 16KJB140003).

REFERENCES

[1] Y. Q. Zhang and D. B. Ge, "A unified FDTD approach for electromagnetic analysis of dispersive objects," *Progress in Electromagnetics Research*, vol. 96, pp. 155-172, 2009.

[2] M. Wang, M. Yu, Z. Xu, et al., "Propagation properties of terahertz waves in a time-varying dusty plasma slab using FDTD," *IEEE Transactions on Plasma Science*, vol. 43, no. 12, pp. 4182-4186, 2015.

[3] A. Guellab and W. Qun, "High-order staggered finite difference time domain method for dispersive Debye medium," *ACES Journal*, vol. 33, no. 4, pp. 430-437, 2018.

[4] W. Shao, X. Ding, and B. Z. Wang, "Efficient sub-gridded FDTD for three-dimensional time-reversed electromagnetic field shaping," *ACES Journal*, vol. 33, no. 8, pp. 828-834, Aug. 2018.

[5] Z. Sun, L. Shi, Y. Zhou, B. Yang, and W. Jiang, "FDTD evaluation of LEMP considering the lossy dispersive ground," *ACES Journal*, vol. 33, no. 1, pp. 7-14, Jan. 2018.

[6] M. R. Cabello, L. D. Angulo, J. Alvarez, A. R. Bretones, and S. G. Garcia, "A new conformal FDTD for lossy thin panels," *IEEE Trans. Antennas Propag.*, vol. 67, no. 12, pp. 7433-7439, Dec. 2019.

[7] A. Taflove and S. C. Hagness, *Computational Electrodynamics: The Finite-difference Time-Domain Method*. 3rd ed., Artech House, Norwood, MA, 2005.

[8] K. S. Yee, "Numerical solution of initial boundary value problems involving Maxwell's equations in isotropic media," *IEEE Trans. Antennas Propagat.*, vol. AP-14, pp. 302-307, 1966.

[9] M. E. Potter, M. Lamoureux, and M. D. Nauta, "An FDTD scheme on a face-centered-cubic (FCC) grids for the solution of the wave equation,"

Journal of Computational Physics, vol. 230, pp. 6169-6183, 2011.

[10] X. Fei, X. H. Tang, and X. J. Zhang, "The construction of low-dispersive FDTD on hexagon," *IEEE Trans. Antennas Propag.*, vol. 53, no. 11, pp. 3697-3703, 2005.

[11] Y. Liu, "Fourier analysis of numerical algorithms for the Maxwell equations," *Journal of Computational Physics*, vol. 124, pp. 396-416, 1996.

[12] M. E. Potter, and M. D. Nauta, "FDTD on face-centered cubic (FCC) grids for Maxwell's equations," *IEEE Trans. Antennas Progag.*, vol. 61, pp. 2116-2122, 2013.

[13] H. Kim, I. S. Koh, and J. G. Yook, "Enhanced total-field/scattered-field technique for isotropic-dispersion FDTD scheme," *IEEE Trans. Antennas Progag.*, vol. 58, no. 10, pp. 3407-3411, 2010.

[14] G. S. Singh, E. L. Tan, and Z. N. Chen, "Analytic fields with higher-order compensations for 3-D FDTD TF/SF formulation with application to beam excitations," *IEEE Trans. Antennas Propagat*., vol. 59, no. 7, pp. 2588-2598, 2011.

[15] T. P. Stefanski, "Application of the discrete Green's function-based antenna simulations for excitation of the total-field/scattered-field interface in the FDTD method," *Microwave and Optical Technology Letters*, vol. 56, no. 8, pp. 1949-1953, 2014.

[16] Y. Zhang, Y. M. Liu, and X. P. Li, "Total-field/scattered-field formulation for FDTD analysis of plane-wave propagation through cold magnetized plasma sheath," *IEEE Trans. Antennas Propag.*, vol. 68, no. 1, pp. 377-387, 2020.

Li Juan Shi received the M.S. degree in Physics from Xidian University, and the Ph.D. degree in Electrical and Mechanical Engineering from Jiangsu University, China, in 2006 and 2014, respectively. Her research interests include electromagnetic scattering and radiation, computational electromagnetism, and electromagnetic field theory.

Li Xia Yang received the Ph.D. in Electronics Engineering from Xidian University, China, in 2004. He is a Professor with the School of Computer Science and Communication Engineering, Jiangsu University, Zhenjiang, China. His research interests include numerical calculation of electromagnetic fields and antenna design.